 doi:10.20944/preprints202209.0379.v1

Communication

Drone Delivery of Dehydro-Sulfurization Utilizing Doubly-Charged Negative Ions of Nanoscale Catalysts Inspired by the Biomimicry of Bee Species' Bio-Catalysis of Pollen Conversion to Organic Honey

Kelvin Suggs [1], Duminda Samarakoon [2], and Alfred Z. Msezane [1*]

[1] Department of Physics and Center for Theoretical Studies of Physical Systems, Clark Atlanta University, Atlanta, Georgia 30314; amsezane@cau.edu; kelvlorenz@yahoo.com
[2] Department of Biological and Physical Sciences, Northwestern State University, Natchitoches, Louisiana 71497; samarakoond@nsula.edu
* Correspondence: A.Z.M. amsezane@cau.edu.; K.S. kelvlorenz@yahoo.com; Tel: 404.819.4188; D.M.; samarakoond@nsula.edu; Tel: 318.357.5225

Abstract: The Sulfur Dioxide (SO_2) compound is a primary environmental pollutant worldwide, whereas elemental Sulfur (S) is a global commodity possessing a variety of industrial as well as commercial functions. The chemical relationship between poisonous SO_2 and commercially viable elemental S has motivated this investigation using Density Functional Theory calculation of the relative transition state barriers for the 2-step Dehydro-sulfurization oxidation-reduction reaction. Additionally, doubly-charged nanoscale platelet Molybdenum Disulfide (MoS_2), Armchair (6,6) Carbon Nanotube, 28-atom Graphene nanoflake (GR-28), and Fullerene C-60 are utilized as catalysts. The optimal heterogeneous and homogeneous catalysis pathways of the 2-step oxidation-reduction from SO_2 to elemental S are further inspired by the biomimicry of the honeybee species multi-step bio-catalysis of pollen conversion to organic honey. Potential applications include environmental depollution, the mining of elemental sulfur, and the functionalization of novel technologies such as the recently patented aerial and amphibious Lynchpin ™ drones.

Keywords: fullerene; graphene; molybdenum disulfide; carbon nanotubes; catalysts; density functional theory; enzymes; honeybee biomimicry; drones; depollution; doubly-charged negative ions

1. Introduction

Environmental depollution and mineral synthesis continue to be areas of international interest given the dynamics of an ever-changing analog-to-digital-to-cloud economy, developing and maintaining sustainable green industrial processes, and future pandemic avoidance [1]. Specifically, elemental S synthesis and SO_2 reduction reactions remain integral to present and future commercial applications as well as adherence to clean environmental protocols [2,3]. Herein, we use Density Functional Theory to investigate the 2-step dehydro-sulfurization reaction. The oxidation-reduction for this 2-step reaction entails increased water molecules between steps one and two with the product of elemental S remaining as the final solute, and molecular water remaining as the solvent within the resulting solution. Therefore, the reaction can efficiently serve a two-fold function, namely as an environmental cleaning agent; while simultaneously creating the commercially profitable elemental S as shown by equations 1 and 2 [4,5].

It has been previously predicted and demonstrated that the experimental application of muon-catalyzed fusion is efficient in tuning chemical reaction barriers due to orbital distortion that accelerates reaction bond breakage. Hence, in this work we extend the experimental muon concept by applying double charged negative ions to nanoscale molecules that also have been previously shown to be efficacious for tuning chemical reaction

 doi:10.20944/preprints202209.0379.v1

[6-8]. Transition metals such as gold, palladium, and silver have been shown previously to be highly inert in the bulk scale. In this theoretical work we overcome the tendency for the chemical inert behavior that is typical of the transition metals by investigating semi-metallic and metallic systems at the nanoscale versus bulk scale as well as exciting the nanoscale catalysts by an electrical charge equivalent to two negative charges. The introduction of doubly-charged negative ions results in single and double bond breakage in the transition state (TS), and bond reformation in the final state or product in the desulfurization redox reaction [9-11]. Hence, we show the intrinsic value of optimizing the 2-step dehydro-sulfurization reaction by the addition of two negative charges to the catalysts Molybdenum Disulfide, Graphene-nanoflake (GR-28), (6,6) Armchair Carbon Nanotube, and Fullerene (C-60) [12]. The varying of homogeneous and heterogeneous nanoscale catalysts in each of the two steps of dehydro-sulfurization reaction is motivated by the novel biomimicry of the fundamental role that the four different enzymes invertase, amylase, glucose oxidase, and catalase play in the bio-catalysis of sucrose conversion to organic honey. We further propose that this study may have future applications in the realm of aero-amphibious drone natural resource mining technologies [13-22].

2. Results

The calculations predict the chemical tunability of 2-step transition state paths of the doubly-charged heterogenous and homogenous nanoscale catalysts for the potential application to toxic SO_2 purification systems [23]. As shown in Table 1 and Table 2, we report Step 1 transition state (TS-1) values of 4.44eV, 1.12eV, 0.49eV, and 0.44eV for CNT (6,6), MoS_2, GR-28, and C-60, respectively. The Step 2 transition state (TS-2) values are 4.36eV, 1.06eV, 4.59eV, 4.30eV for CNT (6,6), MoS_2, GR-28, and C-60, respectively. The introduction of doubly-charged negative ions to the dehydro-sulfurization reaction tunes the transition state reaction barriers of metallic and semi-metallic catalysts yielding calculation results that are consistent with previous international academic and commercial findings [24]. Figure 1 predicts that each step of the 2-Step ORR is optimizable via the sequential heterogenous or homogenous utilization of the doubly-charged negative planar catalysts GR-28 for TS-1 and MoS_2 for TS-2 with the calculated respective relative optimal values of 0.49eV and 1.06eV. However, a similar TS-1 barrier minimization is realized when spherical C-60 and planar MoS_2 are applied sequentially and step-wise with TS-1 and TS-2 predicted to be 0.44eV and 1.06eV [25,26]. Alternatively, catalysis via the homogenous usage of CNT (6,6) is predicted to slow down significantly the reaction speed with values of 4.44eV and 4.36eV for TS-1 and TS-2, respectively. The sole use of the heterogeneous catalyst MoS_2 is to minimize the transition states to 1.12eV for TS-1 and 1.06eV for TS-2. These calculations support the application of the short-lived ion creation fundamental mechanism to multistep chemical reactions. The transition state barriers presented here suggest efficacy for reaction barrier optimization or “chemical tuning" for future depollution and elemental S acquisition applications [27].

The desulfurization reaction mechanism may serve as the fundamental process that mimics honeybee bio-catalysis. Moreover, the focus of this work is desulfurization that entails toxic SO_2 elimination with the simultaneous generation of the elemental Sulfur commodity rather than organic honey production. It is interesting to note that the mechanism for the biochemical production of honey is documented as an approximated 4-step biocatalytic process involving the four primary enzymes invertase, amylase, glucose oxidase, and catalase as presented in figures 8-10[20,21]. The studied catalysts here are analogously tailored to the 2-step desulfurization reaction in lieu of SO_2 elimination with simultaneous generation of elemental Sulfur thereby mimicking the varying of enzymes per each step of the bio-catalysis of organic honey.

2.1. Figures

Preprints (www.preprints.org) | NOT PEER-REVIEWED | Posted: 26 September 2022 doi:10.20944/preprints202209.0379.v1

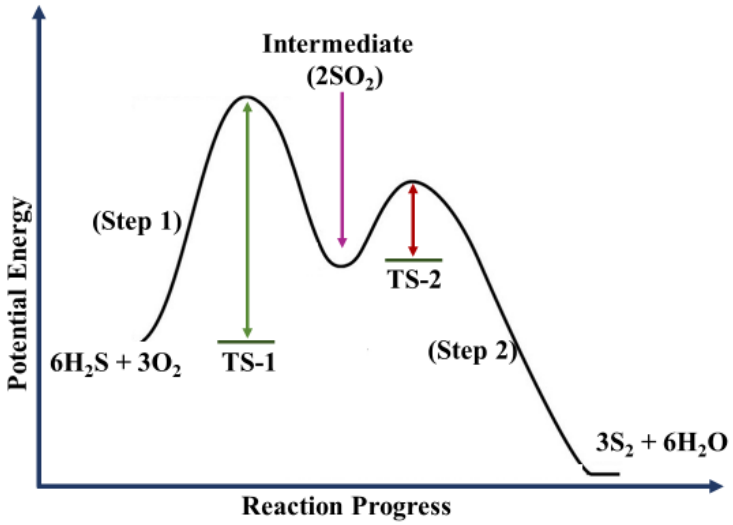

Figure 1. Conceptual rendition of the theoretical 2-step transition state reaction path for the dehydro-sulfurization reaction. The black curve indicates net chemical results from equations 1 and 2 where the activation energies (TS-1) and (TS-2) are the 2-transition state (TS) barriers calculated by ΔTS = TS-initial state for barrier height values for each step represented by the green and Remove "dark" red arrows respectively. The purple arrow represents the intermediate formation of 2 molar sulfur dioxide.

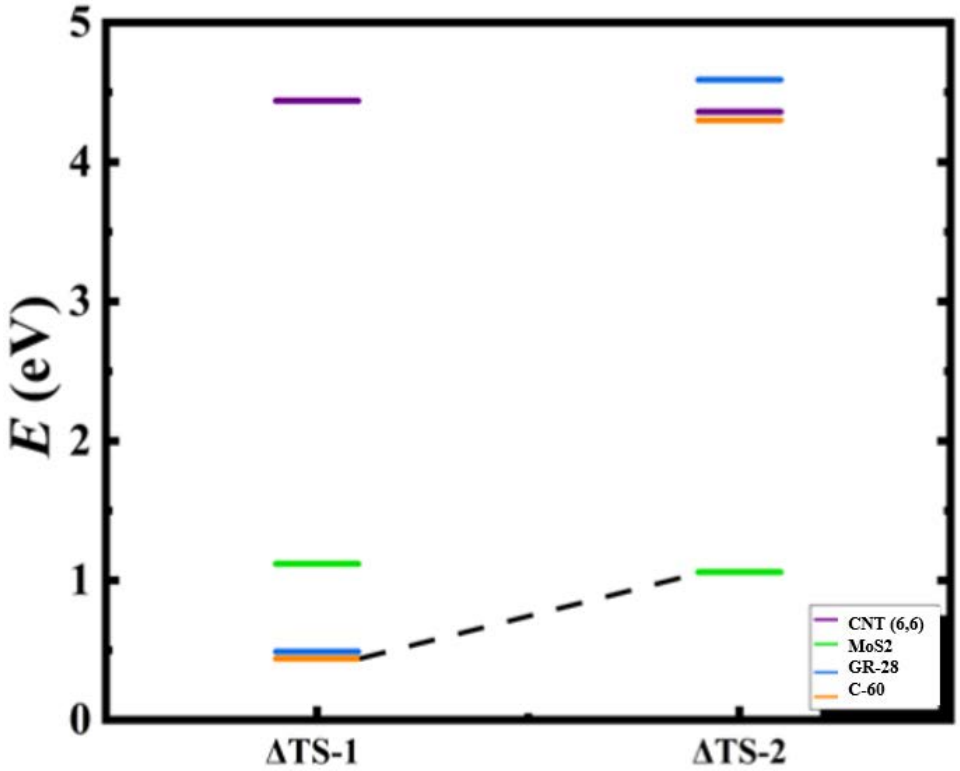

Figure 2. Calculated relative transition state barrier paths values for the 2-Step Oxidation-Reduction Reaction (ORR) of Sulfur dioxide by utilizing Armchair (6,6) Carbon Nanotube, Molybdenum Disulfide (MoS_2), 28-atomed graphene nanoflake (GR-28), and Fullerene (C-60) as catalysts represented by the inset purple, green, blue, and orange bars, respectively. The black dashed line identifies the optimal catalytic path for the transition states 1 and 2. The relative transition state barriers (ΔTS-1) and (ΔTS-2) for the respective Steps 1 and 2 are defined by equation (3): ΔTS=Transition State – Initial State.

Preprints (www.preprints.org) | NOT PEER-REVIEWED | Posted: 26 September 2022 doi:10.20944/preprints202209.0379.v1

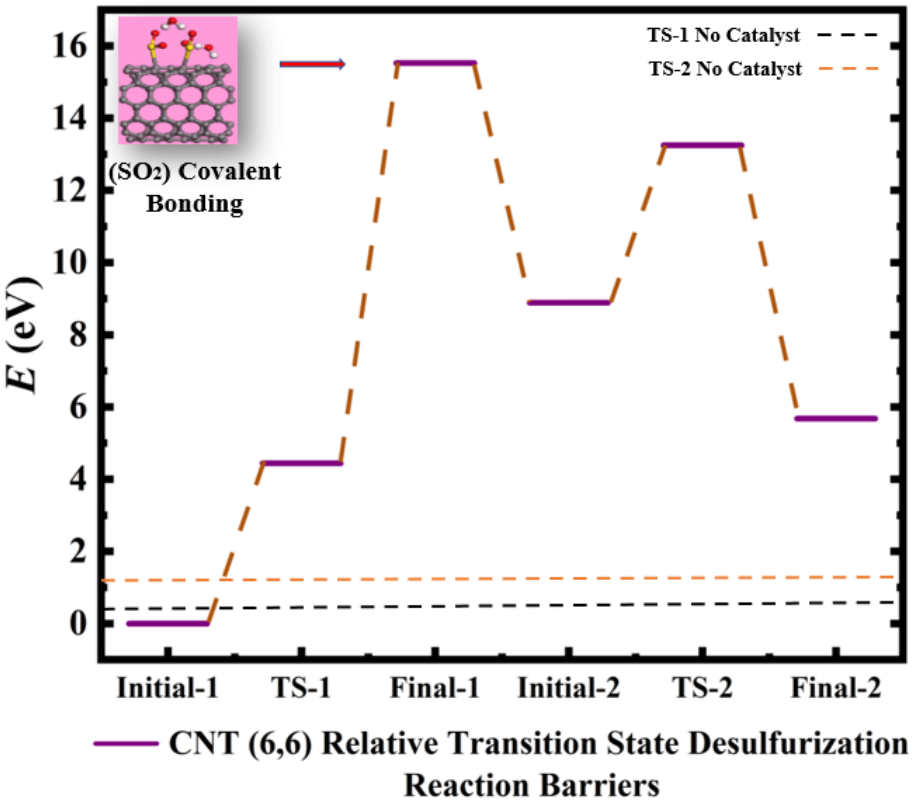

Figure 3. Calculated relative initial, transition, and final states reaction barriers of Step-1 and Step-2 for the oxidation reduction of Sulfur dioxide to elemental Sulfur utilizing Armchair Carbon Nanotube CNT (6,6) represented by the purple bars. Pink Inset: Geometrically optimized Final State 1 (Final-1) of SO_2 covalently bonding to CNT (6,6) surrounded by 2 water molecules. Sulfur, Carbon, Oxygen, and Hydrogen are represented by the yellow, gray, red, and white spheres, respectively.

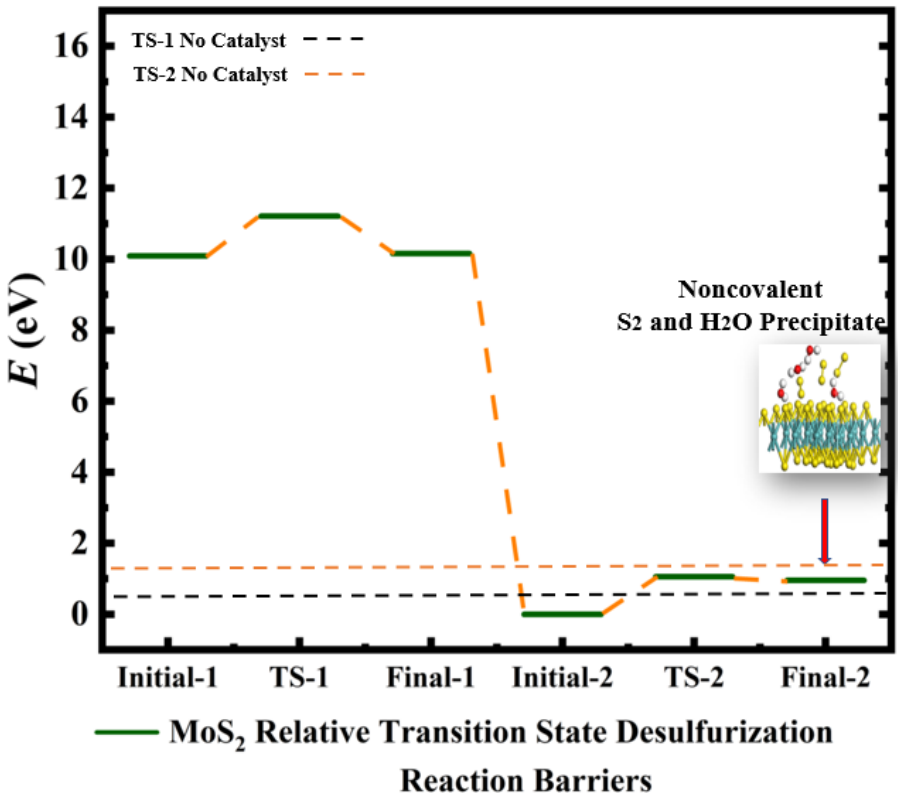

Preprints (www.preprints.org) | NOT PEER-REVIEWED | Posted: 26 September 2022 doi:10.20944/preprints202209.0379.v1

Figure 4. Calculated relative initial, transition, and final states reaction barriers of Step-1 and Step-2 for the oxidation reduction of Sulfur dioxide to elemental Sulfur by utilizing the doubly-charged catalyst MoS_2 represented by the dark green bars. White Inset: Geometrically optimized Final State 2 (Final-2) of MoS_2 with noncovalent precipitated S_2 and H_2O. Sulfur, Carbon, Oxygen, and Hydrogen are represented by the yellow, gray, red, and white spheres, respectively.

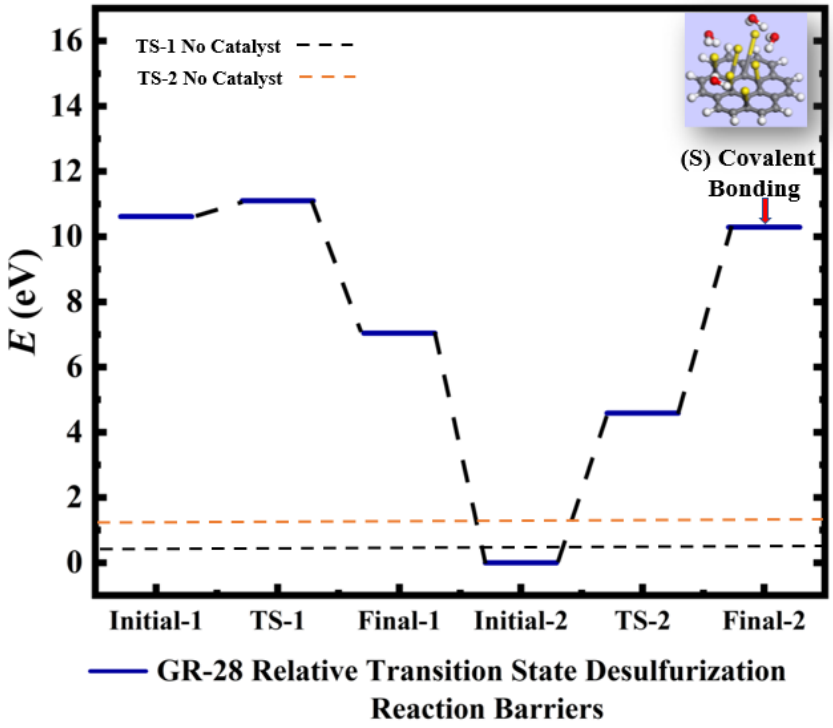

Figure 5. Calculated relative initial, transition, and final states reaction barriers of Step-1 and Step-2 for the oxidation reduction of Sulfur dioxide to elemental Sulfur (S) by utilizing doubly-charged catalyst graphene flake (GR-28) represented by the blue bars. Light Blue Inset: Geometrically optimized Final State 2 (Final-2) of GR-28 with covalent bonded atomic S surrounded by 4 molar H_2O. Sulfur, Carbon, Oxygen, and Hydrogen are represented by the yellow, gray, red, and white spheres, respectively.

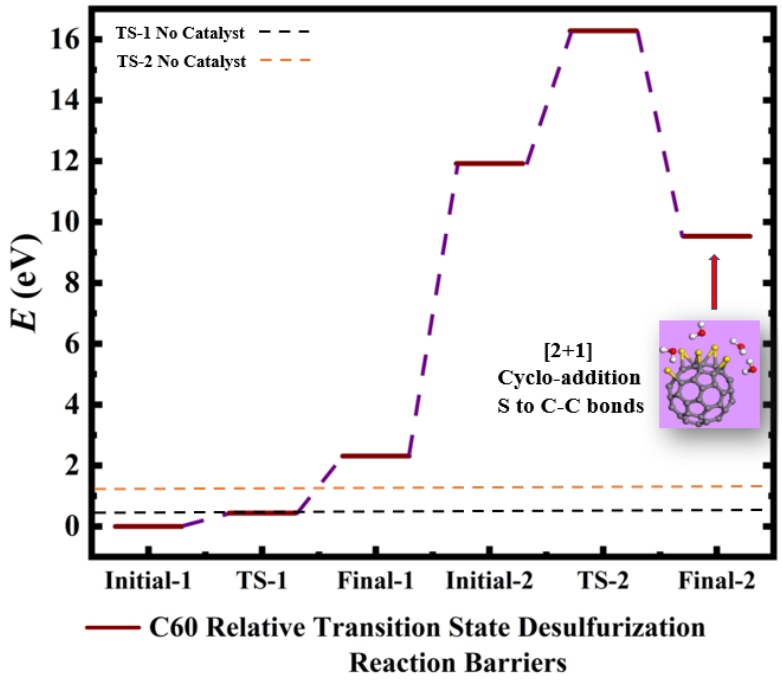

Preprints (www.preprints.org) | NOT PEER-REVIEWED | Posted: 26 September 2022 doi:10.20944/preprints202209.0379.v1

Figure 6: Calculated relative initial, transition, and final states reaction barriers of Step-1 and Step-2 for the oxidation reduction of Sulfur dioxide to elemental Sulfur (S) by utilizing doubly-charged negative fullerene C-60 represented by the brown bars. Light Purple Inset: Geometrically optimized Final State 2 (Final-2) of the C-60 catalyst with [2+1] cycloaddition elemental S to fullerene C-C bonds and 4 molar H_2O as the final product for Step-2. Sulfur, Carbon, Oxygen, and Hydrogen are represented by the yellow, gray, red, and white spheres, respectively.

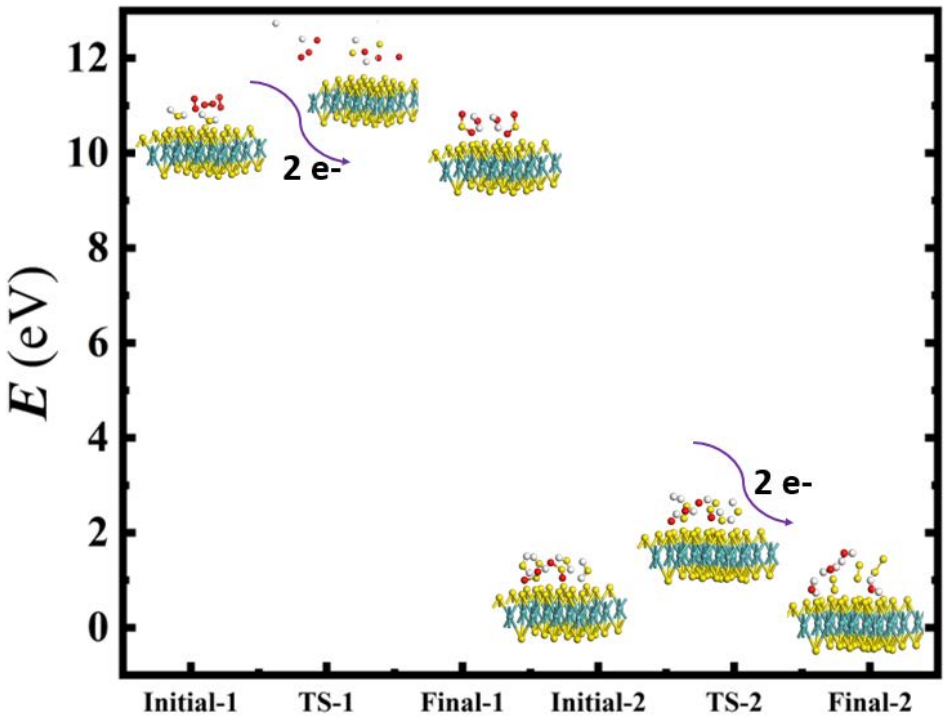

Figure 7. Calculated initial, transition, and final states for geometrically optimized doubly-charged negative AA stacked MoS_2 catalyzing the oxidation reduction of Sulfur dioxide to elemental Sulfur. The Mo, S, O, and H atoms are represented by cyan, yellow, red, and white spheres, respectively. The curved arrows demonstrate the introduction of 2 electrons into the reactant states causing bond breakage in the predicted transition states of Step 1 and Step 2 which describes the doubly-charged catalytic process used for our calculations.

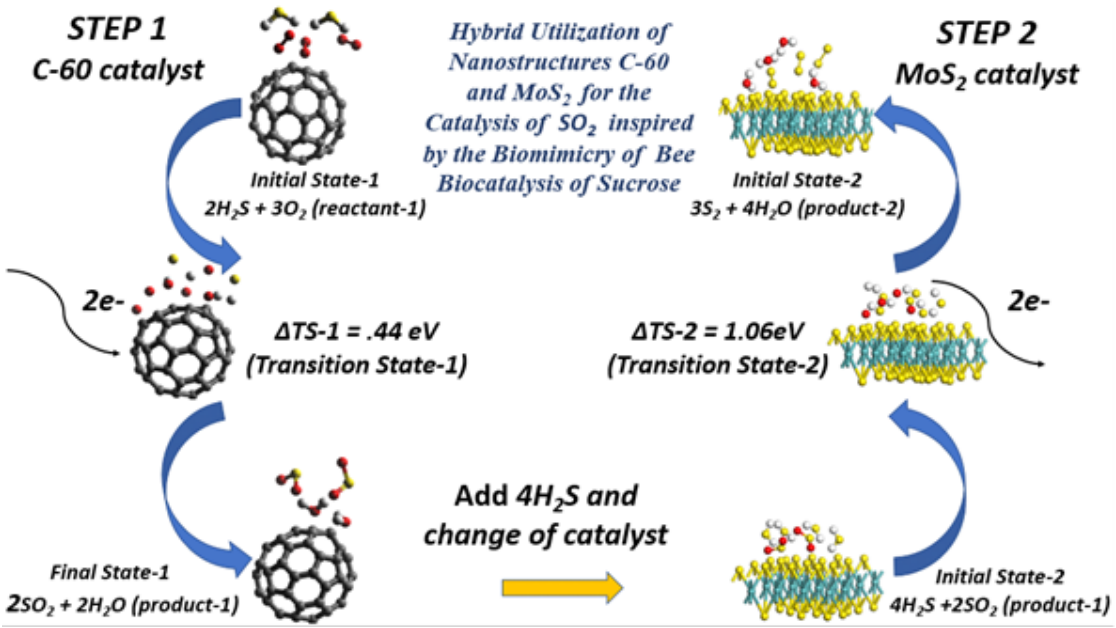

Preprints (www.preprints.org) | NOT PEER-REVIEWED | Posted: 26 September 2022 doi:10.20944/preprints202209.0379.v1

Figure 8. Bee biomimicry inspired rendering of both Steps of the initial, transition, and final states for geometrically optimized doubly- charged fullerene C-60 and AA stacked MoS_2 heterogeneously catalyzing the oxidation reduction of Sulfur dioxide to elemental Sulfur. The Mo, S, O, and H atoms are represented by cyan, yellow, red, and white spheres, respectively. The curved arrows demonstrate the introduction of 2 electrons into the reactant states causing bond breakage in the predicted relative transition states of Step 1 and Step 2.

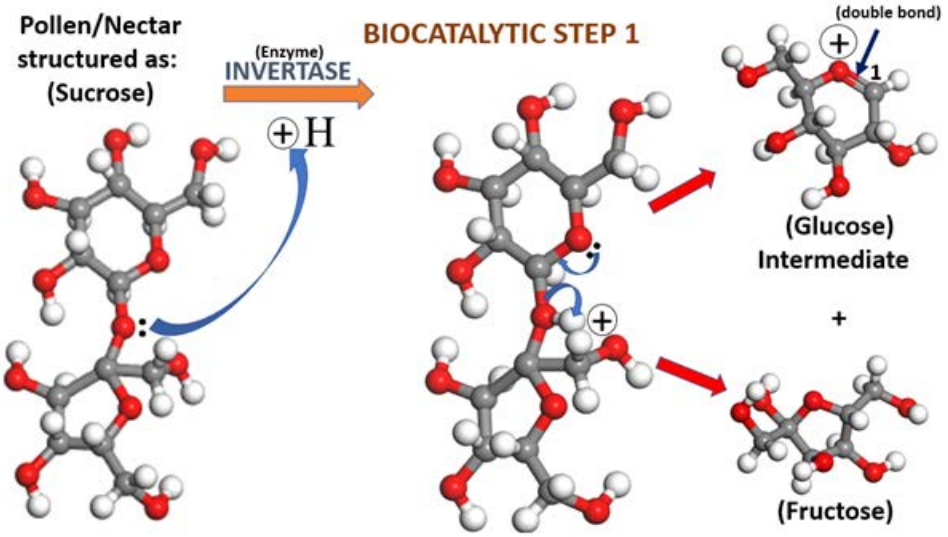

Figure 9. The biocatalytic Step 1 conversion of the Sucrose molecule ($C_{12}O_{11}H_{22}$) contained in nectar and pollen to intermediate glucose ($C_6O_5H_{11}$) and fructose molecules ($C_6H_{12}O_6$). The orange arrow indicates the utilization of the enzyme invertase as the biocatalytic promoter of the reaction. The blue arrows indicate the flow of two electrons that cause bond breakage and reformation. The gray, red, and white spheres represent Carbon, Oxygen, and Hydrogen, respectively. The red arrows indicate the generation of glucose intermediate and fructose molecules after the application of Invertase and bond breakage from Sucrose.

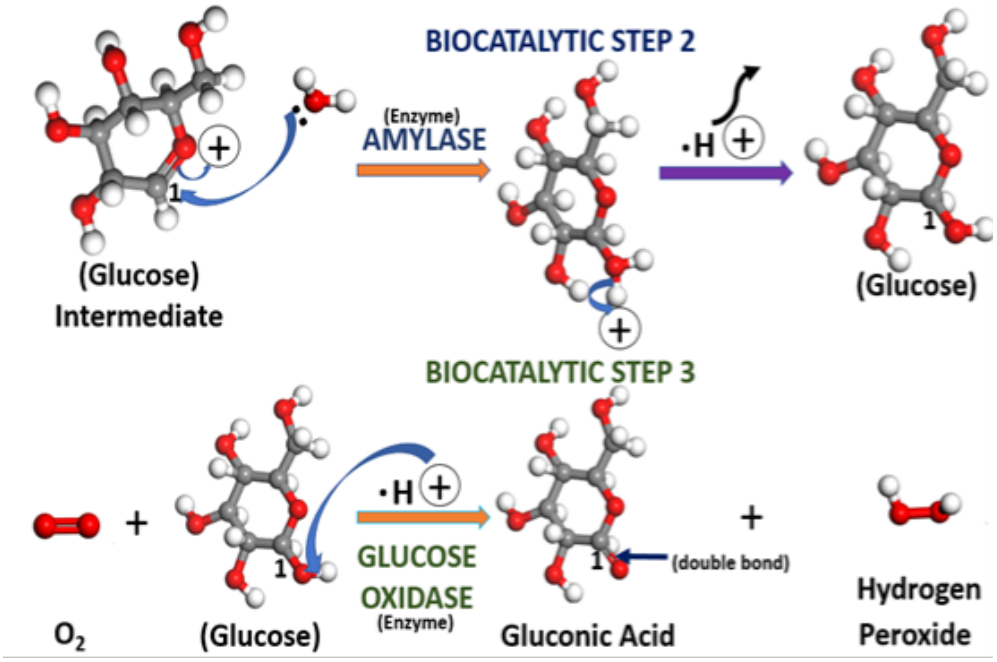

Figure 10. The Step 2 and Step 3 mechanisms for glucose intermediate decomposition to glucose and the oxidation of glucose ($C_6H_{12}O_6$) to gluconic acid ($C_6H_{11}O_6$) and hydrogen peroxide. Step 2 uses the enzyme amylase whereas Step 3 has the enzyme glucose oxidase as the promotor of the reaction. The index "1" is used to indicate the position of the C=O double bond throughout the mechanism. The gray, red, and white spheres represent Carbon, Oxygen, and Hydrogen, respectively.

Preprints (www.preprints.org) | NOT PEER-REVIEWED | Posted: 26 September 2022 doi:10.20944/preprints202209.0379.v1

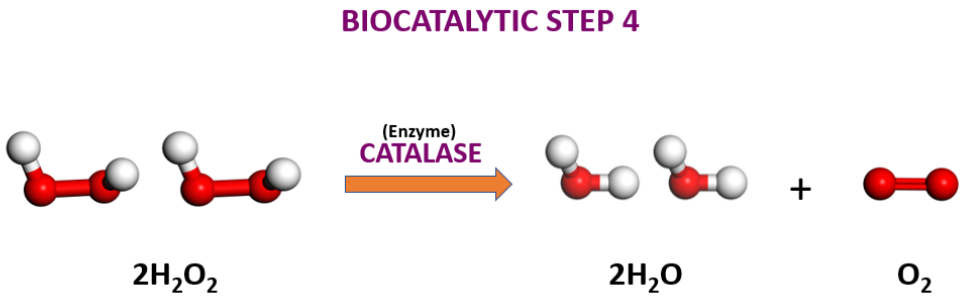

Figure 11. The Step 4 of the final step of the sucrose conversion to organic honey. The enzyme catalase decomposes 2 molar hydrogen peroxide to 2 molar water and diatomic oxygen. The red and white spheres represent Oxygen and Hydrogen, respectively.

2.2. Tables

Table 1. Direct comparison of the calculated relative transition state barrier differential heights from initial states (ΔTS =TS-initial state) for Steps 1 and 2 of the oxidation reduction reaction to atomic Sulfur are represented by ΔTS-1 and ΔTS-2 in electron-volts (eV). Armchair (6,6), carbon nanotube (CNT (6.6)), Molybdenum disulfide (MoS_2), graphene flake containing 28 atoms (GR-28), and fullerene (C-60) are the doubly-charged catalysts.

Catalyst (Doubly-Charged)	ΔTS-1 (eV)	Barrier (%) Change (TS-1)	ΔTS-2 (eV)	Barrier (%) Change (TS-2)
CNT (6,6)	4.44	92.6	4.36	73.2
MoS_2	1.12	70.5	1.06	-10.4
GR-28	0.49	32.7	4.59	74.5
C-60	0.44	25	4.30	72.8
Doubly-charged only	0.33	0	1.17	0

Table 2. Calculated relative initial, transition, and final states in electron-volts (eV) of Step 1 and Step 2 of the desulfurization redox reaction. The relative states have been calibrated to zero for the lowest calculated potentials that were found in Step 1 "or" Step 2 for Armchair (6,6) carbon nanotube, Molybdenum disulfide (MoS_2), graphene flake containing 28 atoms (GR-28), and fullerene (C-60) doubly-charged catalysts. The calculations performed without the assistance of a catalyst for ΔTS-1 and ΔTS-2 are presented as (doubly- charged only) for the introduction of 2e-.

Catalyst (Doubly-Charged)	Initial 1 (eV)	TS-1 (eV)	Final 1 (eV)	Initial 2 (eV)	TS-2 (eV)	Final 2 (eV)
CNT (6,6)	0	4.44	15.34	8.89	4.36	5.68
MoS_2	10.09	11.21	10.16	0	1.06	0.95
GR-28	10.62	11.10	7.05	0	4.59	10.29
C-60	0	0.44	2.31	11.92	4.30	9.53
Doubly- charged only	0	0.33	0.31	0.19	1.17	1.09

 doi:10.20944/preprints202209.0379.v1

3. Discussion

The dehydro-sulfurization reaction is an oxidation reduction mechanism (ORM) also referred to as redox reaction. The reactant includes the introduction of diatomic oxygen into Sulfur dihydride. Our research approach further introduces 2 electrons into the chemical reaction in order to increase the catalytic reactivities of heterogeneous (moly-disulfide) MoS_2 as well as the homogeneous molecules armchair (6,6) carbon nanotube, fullerene (C-60), and graphene (Gr-28). The resulting product is Sulfur dioxide precipitated in 2 molar waters due to bond breakage and reformation as indicated by equation 1. Additionally, 2 more electrons are added to the catalysts in order to further break the bond arrangements of the reactant in step 2 containing Sulfur dihydride and 2 molar Sulfur dioxide. Hence, the oxygen is removed from the Sulfur dioxide due to bond breakage to form 3 molar diatomic sulfurs and 4 molar waters in the final product of step 2. The addition of doubly-charged negative ions to the spherical, cylindrical, and planar nanoscale catalysts function as a "chemical tuning" agent for each step of the dehydro-sulfurization reaction [28]. Moreover, the varying of the catalysts with each step of the redox reaction mimics the biocatalytic mechanism of sucrose conversion to organic honey through the flow of 2e- electrons that similarly cause bond breakage and bond reformation as shown in figures 8-10. The relative barriers generated by the 2e- electrons addition are compared with reference to the initial states according to equation 3. The 2-step chemical reaction can therefore be tailored with various levels of control at each step of the reaction by the sequential application of homogeneous and/or heterogeneous catalysts as indicated by figures 1-7. The percentage barrier changes are calculated with equation 5, and are presented in table I showing that the reaction barriers are increased in figure 3 by 92.6% and 73.2% for CNT (6,6) calculations of TS-1 and TS-2, respectively. Hence, CNT (6,6) catalysts are predicted to slow the rate of reaction as a substrate for desulfurization. However, MoS_2 is calculated to have a barrier increase of 70.5% for TS-1 and a barrier decrease of –10.2% as shown in figure 4 which indicates that MoS_2 is predicted to be an excellent accelerator of reaction for Step 2 of desulfurization. Figure 5 illuminates that Gr-28 tends to slow the desulfurization reaction by 32.7% and 74.5% for TS-1 and TS-2, respectively. C-60 is calculated to have the lowest reaction impedance of 25% for Step-1 as presented in Figure 6. However, for Step-2 the reaction barrier is reported to be 72.8%. Figure 8 shows the respective calculated transition state energies and geometrically optimized view of the catalysis steps when C-60 and MoS2 catalysts are applied to Step-1 and Step-2 respectively. The two materials are predicted to effectively maintain or lower transition state barriers when applied sequentially. C-60 changes the barrier by 25%, whereas MoS2 reduces the transition state energy by -10.4% according to Table 1. Figures 9-11 are geometrical optimizations of the pollen conversion to organic honey mechanism that honey bees use wherefore the enzymes invertase, amylase, glucose oxidase, and catalase are applied in nature for honey production. Similarly, the enzymes are initiated by the flow of 2e-. We therefore have applied two varying inorganic molecules to each step of the reaction rather than applying the catalysts uniformly to all steps. This approach may find efficacy in the optimization to a plethora of other multi-step reactions.

Equations:

Catalyst (-2)

1) $2H_2S + 3O_2 \xrightarrow{\text{------}} 2SO_2 + 2H_2O$ **STEP 1**

Catalyst (-2)

2) $4H_2S + 2SO_2 \xrightarrow{\text{------}} 3S_2 + 4H_2O$ **STEP 2**

_____

 doi:10.20944/preprints202209.0379.v1

3) $6H_2S + 3O_2$ -------> $3S_2 + 6H_2O$ **("Net" Chemical Results for the Reaction)**

4) **ΔTS = Transition State - Initial State (Relative T.S. Reaction Barriers)**

5) $\frac{TS-std}{TS}\ x\ 100\%$ **= (Barrier percentage change given reaction standard)**

4. Materials and Methods

[2+1] Cyclo-addition is a typical phenomenon that occurs in organo-metallic catalytic systems, oxidation reduction reactions, and nitrene chemistry. In this work, [2+1] Cyclo-addition is specifically used in the geometrical optimization of fullerene C-60 as shown in the inset of Figure 5 [29,30]. However, 28-atomed graphene (GR-28), Armchair Nanotube (6,6), and MoS_2 catalysts are geometrically optimized by covalent and noncovalent bonding as indicated in the insets of Figures 2-5 and the entirety of Figures 4-6. The doubly-charged MoS_2, GR-28, CNT (6,6), and C-60 catalysis substrates function as reaction barrier tuning mechanisms for the desulfurization oxidation reduction reaction (ORR) as indicated in equations 1 and 2[28-31]. Oxidation-reduction speed is therefore predicted to be regulated by the size, type, and charge of any given sample of catalysts used to produce the elemental Sulfur and water products for both steps of the reaction. Hence, the quality, quantity, and overall efficiencies of the reactions can be tailored to the reactivity of each step of the ORR reaction as well as the type of nanoscale catalyst that is used [32-35]. Transition state theory is executed by performing Density Functional Theory approximations shown to be excellent for predicting chemical, physical, and electromagnetic properties of nanoscopic systems. The initial, transition, and final states are optimized, and are dependent on the application of two negative charges that activate the metallic and semi-metallic planar, cylindrical, and spherical catalysts that cause single and double bond breakage in the transition state consistent with the research findings [36]. The GR-28 nano-flake configuration investigated is due to its similar geometrical structure and chemical function as the "Sulflower" discussed in the 2017 "MOLECULES OF THE YEAR" edition of the C&EN journal [37,38]. Geometrical optimization calculation efficiency for initial, transition, and final states is achieved, as indicated by the data in Table 2, with the usage of minimum basis sets and Self-Consistent Field (SCF) tolerances of 0.01Ha, and smearing values of 0.05Ha. We use Equation (3) in order to specifically compare the relative Transition State (ΔTS) values in Table 1 in order to highlight the most likely efficient heterogenous or homogenous catalyst configuration as indicated in Figure 1[39,40]. Whereas, Figures 2-5 show that the calculated relative reaction barriers for the initial, transition, and final states are zeroed to the minimum potential for initial state calculated values occurring in Step 1 or Step 2 for each set of nanoscale catalysts. A 3-D triclinic lattice type with lattice lengths a:12.7548, b:12.7548, and c:17.2744 Angstroms with subsequent respective angles consisting of α:90, β:90, μ: 120 degrees is used for the AA stacked MoS_2 catalyst. The values of the MoS_2 are represented by a 1x1x1 Monkhorst-Pack grid as shown in the inset of Figure 3 as well as the entirety of Figure 6. Noncovalent bonding is used to predict TS-1 and TS-2 for MoS_2 versus the Cyclo-addition and covalent approaches utilized for CNT (6,6), GR-28, and C-60[41-44].

5. Conclusions

The transition states for spherical C-60, planar MoS_2 and graphene (Gr-28), and CNT (6,6) tubal shaped have been calculated. The results indicate efficacy for the chemical tuning of the dehydro-sulfurization reaction as inspired by nature's biocatalytic solution to the biocatalytic conversion of pollen or nectar to organic honey. We further propose that

our findings may assist in the understanding and development of future innovative technologies by utilizing tangential flight enabled amphibious Lynchpin ™ drones as patented and developed by T. Dashawn Howard et.al. Some unique capabilities of the patented drone technology include aerial bird-like flock, bee swarm, and "school" of fish biomimicry that is tailorable to future multidisciplinary engineering solutions. For example, we postulate that the implementation of our doubly-charged negative-ion catalytic desulfurization predictions combined with the Lynchpin ™ drone design may offer promising SO_2 depollution remedies as well as the profitable commercial mining of elemental Sulfur [8,20,45].

6. References

1. Hu, Y.-L.; Zhu, H.-R.; Wei, S.H. Single-doped charged gold cluster with highly selective catalytic activity for the reduction of SO_2 by CO: First-principles study. Chin. Phys. B 2019, 28, 113101. DOI:10.1088/1674-1056/ab4cdd
2. Liu, Donghua; Shenggang Ren; Li, Wenming; "SO_2 emissions trading and firm exports in China." *Energy Economics* (2022): 105978. DOI: https://doi.org/10.1016/j.eneco.2022.105978.
3. J. Socha; P. Gruba; and M. Pietrzykowski. The Current State of Environmental Pollution with Sulfur Dioxide (SO_2) in Poland Based on Sulfur Concentration in Scots Pine Needles. Environmental Pollution. 2020, 258, 113559; DOI: https://doi.org/10.1016/j.envpol.2019.113559.
4. Denis, Pablo A.; Iribarne, Federico. "New Approach to Accomplish the Covalent Functionalization of Boron Nitride Nanosheets: Cycloaddition Reactions". The Journal of Physical Chemistry C 2018, *122* (32), 18583-18587. DOI: https://doi.org/10.1021/acs.jpcc.8b05907
5. Pablo A., Denis; Iribarne, Federico. "Cycloaddition Reactions between Graphene and Fluorinated Maleimides". The Journal of Physical Chemistry C 2017, *121* (24), 13218-13222. DOI: https://doi.org/10.1021/acs.jpcc.7b03413
6. Felfli, Z.; Suggs, K.; Nicholas, N.; Msezane, A.Z. Fullerene negative ions: Formation and catalysis. Int. J. Mol. Sci. 2020, 21, 3159. DOI: 10.3390/ijms21093159
7. Kelvin Suggs, Filmon Kiros, Aaron Tesfamichael, Zineb Felfli and Alfred Z Msezane; Charge modification of metal atoms: Catalysis of Water to Peroxide September 2015 Journal of Physics Conference Series 635(5):052018 DOI:10.1088/1742-6596/635/5/052018
8. Michael; Schnitzer, Rafael; Science, Doubly Charged Negative Atomic Ions of Hydrogen, 6 Feb 1976, Vol 191, Issue 4226, pp. 463-464, DOI: 10.1126/science.191.4226.463A HYPERLINK "https://www.science.org/doi/10.1126/science.191.4226.463" HYPERLINK
9. Zhongying Wang and Baoxia Mi, Environmental Applications of 2D Molybdenum Disulfide (MoS2) Nanosheets Environmental Science & Technology 2017 51 (15), 8229-8244DOI: 10.1021/acs.est.7b01466
10. Kroto, H. The stability of the fullerenes Cn, with n = 24, 28, 32, 36, 50, 60 and 70. Nature 329, 529–531 (1987). https://doi.org/10.1038/329529a0
11. Moosavi-Khoonsari, Elmira; Van Ende, Marie-Aline; Jung, In-ho. "Kinetic simulation of hot metal pretreatment: desulfurization using powder injection." *Metallurgical and Materials Transactions B* (2022): 1-18. DOI: https://doi.org/10.1007/s11663-022-02 HYPERLINK "https://doi.org/10.1007/s11663-022-02437-1"437-1
12. Suggs, Kelvin; Reuven, Darkeyah; Wang, Xiao; "Electronic properties of cycloaddition-functionalized graphene." The Journal of Physical Chemistry C 115.8 (2011): 3313-3317. DOI: 10.1021/JP111637B
13. Dunnington, Lucila; Nakagawa, Musami; Fast and safe gas detection from underground coal fire by drone fly over, Environmental Pollution, Vol. 229, 2017, pp. 139-145, ISSN 0269-7491, https://doi.org/10.1016/j.envpol.2017.05.063.
14. Shahmoradi, Javad; Talebi, Elaheh; Roghanchi, Pedram; Hassanalian; A Comprehensive Review of Applications of Drone Technology in the Mining Industry, *Drones* 2020, *4*(3), 34, **https://doi.org/10.3390/dr HYPERLINK "https://doi.org/10.3390/drones4030034"ones4030034**
15. Hassanalian, M.; Abdelkefi, A.; Classifications, applications, and design challenges of drones: A review, Progress in Aerospace Sciences, Volume 91, 2017, Pages 99-131, ISSN 0376-0421, https://doi.org/10.1016/j.paerosci.2017.04.003.
16. Riddle, Sarah; The Chemistry of Honey | Bee Culture 'The Magazine of America Beekeeping"; JULY 2016
17. Jung, Dirk; Streb, Carsten; Hartmann, Martin; Covalent Anchoring of Chloroperoxidase and Glucose Oxidase on the Mesoporous Molecular Sieve SBA-15, Int. J. Mol. Sci. 2010, 11(2), 762-778; https://doi.org/10.3390/ijms11020762
18. Billingsley, Ethan J.; Ghommem, Mehdi; Vasconcellos, Rui; Abdelkefi, Abdessattar; Biomimicry and Aerodynamic Performance of Multi-Flapping Wing Drones Published Online:4 Jan 2021 https://doi.org/10.251 HYPERLINK "https://doi.org/10.2514/6.2021-0227"4/6.2021-0227
19. J. Socha; P. Gruba; and M. Pietrzykowski. The Current State of Environmental Pollution with Sulfur Dioxide (SO_2) in Poland Based on Sulfur Concentration in Scots Pine Needles. Environmental Pollution. 2020, 258, 113559; DOI: https://doi.org/10.1016/j.envpol.2019.113559.
20. Liu, Donghua; Shenggang Ren; Li, Wenming; "SO_2 emissions trading and firm exports in China." *Energy Economics* (2022): 105978. DOI: https://doi.org/10.1016/j.eneco.2022.105978.

21. Denis, Pablo A.; Iribarne, Federico. "New Approach to Accomplish the Covalent Functionalization of Boron Nitride Nanosheets: Cycloaddition Reactions". The Journal of Physical Chemistry C 2018, *122* (32), 18583-18587. DOI: https://doi.org/10.1021/acs.jpcc.8b05907
22. Pablo A., Denis; Iribarne, Federico. "Cycloaddition Reactions between Graphene and Fluorinated Maleimides". The Journal of Physical Chemistry C 2017, *121* (24), 13218-13222. DOI: https://doi.org/10.1021/acs.jpcc.7b03413
23. Xu, Chi, et al. "Heteroatom-doped monolithic carbocatalysts with improved sulfur selectivity and impurity tolerance for H2S selective oxidation." *ACS Catalysis* 11.14, 2021, 8591-8604, DOI: 10.1021/acscatal.1c01252
24. Shafiq, Iqrash; Shafique, Sumeer; Akhter, Parveen; Yang, Wenshu; Hussain, Murid (2020-06-23). "Recent developments in alumina supported hydrodesulfurization catalysts for the production of sulfur-free refinery products: A technical review". Catalysis Reviews. 64: 1–86. doi:10.1080/01614940.2020.1780824. ISSN 0161-4940.
25. B. Delley; An all-electron numerical method for solving the local density functional for polyatomic molecules. J. Chem. Phys. 92, 508 (1990). DOI: https://doi.org/10.1063/1.458452
26. B. Delley; From molecules to solids with the DMol3 approach, J. Chem. Phys. 113, 7756 (2000). DOI: https://doi.org/10.1063/1.1316015
27. Suggs, K.; Msezane, A.Z.; Doubly-Charged Negative Ions of Triple-Hybrid Atomic-Metal, Super-benzene, Fullerene, and Nanotube as Novel Catalysts for Clean Air through SO_2 Reduction by CO. *Preprints* 2021, 2021060265
28. Ruquan Ye, Dustin K. James, and James M. Tour, Laser-Induced Graphene, Accounts of Chemical Research 2018 51 (7), 1609-1620, DOI: 10.1021/acs.accounts.8b00084
29. Ajayan, P., Tour, J. Nanotube composites. Nature 447, 1066–1068 (2007). https://doi.org HYPERLINK "https://doi.org/10.1038/4471066a"/10.1038/4471066a
30. Yang, Jiaqi; Chen, Junfeng; Wang Xuemei; Yang, Daoxin, Zhang, Yiwen; Wu, Yiqun; Zhao, Yongyue; Wang,Yongle; Wei, Qingying; Wang, Renjun; Liu, Yanyan; Yang, Yuewei; Improving oxygen reduction reaction of microbial fuel cell by titanium dioxide attaching to dual metal organic frameworks as cathode, Bioresource Technology, Volume 349,2022,126851, ISSN 0960-8524, DOI: https://doi.org/10.1016/j.biortech.2022.126851
31. Hu, Feiyang, et al. "Graphene aerogel supported Ni for CO2 hydrogenation to methane." *Industrial & Engineering Chemistry Research* 60.33, 2021,12235-12243. DOI: 10.1021/ACS.IECR.1C01953
32. Jin, Chengkai, et al. "Adsorption of Transition-Metal Clusters on Graphene and N-Doped Graphene: A DFT Study." *Langmuir* 38.12, 2022, 3694-3710. DOI: 10.1021/ACS.LANGMUIR.1C03187
33. Cristol, S., et al. "Theoretical study of the MoS2 (100) surface: a chemical potential analysis of sulfur and hydrogen coverage." *The Journal of Physical Chemistry B* 104.47, 2000, 11220-11229. https://doi.org/10.1021/jp0023819;
34. Li, Yuan, et al. "Theoretical analysis of selective catalytic oxidation of H2S on Fe-N3 co-doped graphene." *Molecular Catalysis* 524, 2022, 112318, *DOI: 10.1016/j.mcat.2022.112318*
35. Wang, H., Chen, L., Lv, Y., Liu, J. and Feng, G. 'A first principle comparative study on chemisorption of [H.sub.2] on [C.sub.60], [C.sub.80], and [Sc.sub.3]N@[C.sub.80] in gas phase and chemisorption of [H.sub.2] on solid phase [C.sub.60]', *Journal of Nanomaterials* 2014, https://link.gale.com/apps/doc/A423500465/AONE?u=anon~bdd95645&sid=googleScholar&xid=e1c1bf6a, DOI: 10.1155/2014/676908
36. Chen, Xin, Fan Ge, and Nanjun Lai. "Probing the catalytic activity and poisoning-tolerance ability of endohedral metallofullerene Fen@ C60 (n= 1− 7) catalysts in the oxygen reduction reaction." *Journal of The Electrochemical Society* 167.2, 2020, 024515, *DOI: 10.1149/1945-7111/ab6cf1*
37. Ritter, S.K.; MOLECULES OF THE YEAR C&EN highlights some of the coolest compounds reported in 2017: "A New Sulflower Bloomed". https://cen.acs.org/articles/95/i49/molecules-of-the-year2017.html; DOI: 10.1039/c7cc06273g
38. 10. R. Dong; M. Pfeffermann; D. Skidin; F. Wang; Y. Fu; A. Narita; M. Tommasini; F. Moresco; G. Cuniberti; R. Berger; K. Müllen; X. Feng. Persulfurated Coronene: A New Generation of "Sulflower". Journal of the American Chemical Society 2017 139 (6), 2168-2171 DOI: 10.1021/jacs.6b1263
39. Karatas, Okan; Gengec, Nevin Atalay; Gengec, Erhan; Khataee, Alireza; Kobya, Mehmet, High-performance carbon black electrode for oxygen reduction reaction and oxidation of atrazine by electro-Fenton process, Chemosphere, Volume 287, Part 4,2022,132370, ISSN 0045-6535, DOI: https://doi.org/10.1016/j.chemosphere.2021.132370.
40. Xu, Feng; Cai, Shaobin; Lin, Benfeng; Yang, Lui; Le, Huafeng; Mu, Shichun; Geometric Engineering of Porous PtCu Nanotubes with Ultrahigh Methanol Oxidation and Oxygen Reduction Capability, 24 March 2022, DOI: https://doi.org/10.1002/smll.202107387.
41. Betiha, Mohamed A.; Rabie,Abdelrahman M.; Ahmed, Hoda S.; Abdelrahman, Asmaa A.; F.El-Shahat, Mohammed; Oxidative desulfurization using graphene and its composites for fuel containing thiophene and its derivatives: An update review Egyptian Journal of Petroleum Volume 27, Issue 4, December 2018, Pages 715-730, DOI: https://doi.org/10.1016/j.ejpe.2017.10.006
42. Gómez Martínez, Melania; Buxaderas, Perez de Armiñan, Eduardo; Pastor, Isidro; Alonso, Diego; Palladium nanoparticles supported on graphene and reduced graphene oxide as efficient recyclable catalyst for the Suzuki-Miyaura reaction of potassium aryltrifluoroborates Dedicated to the memory of Prof. Carlos F. Barbas III., Journal of Molecular Catalysis A: Chemical Aug 2015 10.1016/j.molcata.2015.03.022
43. Maihom, Thana; Sittiwong, Jarinya; Probst, Michael; Limtrakulb, Jumras; Understanding the interactions between lithium polysulfides and anchoring materials in advanced lithium–sulfur batteries using density functional theory Phys. Chem. Chem. Phys., 2022,24, 8604-8623 DOI: https://doi.org/10.1039/D1CP05715D

44. Liao, Xiaobin; Lu, Ruihu; Xia, Lixue; Liu, Qian; Wang, Huan; Zhao, Kristin; Wang, Zhaoyang; Zhao, Yao; Density Functional Theory for Electrocatalysis, 26 April 2021 DOI: https://doi.org/10.1002/eem2.1220 HYPERLINK "https://doi.org/10.1002/eem2.12204"4
45. T Dashawn Howard; https://patents.justia.com/patent/11117065